SO$_2$ emissions during the 2021 eruption of La Soufrière, St Vincent, revealed with back-trajectory analysis of TROPOMI imagery

Ben Esse[1]*, Mike Burton[1], Catherine Hayer[1], Rodrigo Contreras-Arratia[2], Thomas Christopher[2,3], Erouscilla P. Joseph[2], Matthew Varnam[4] and Chris Johnson[5]

[1]COMET, Department of Earth and Environmental Sciences, The University of Manchester, Manchester M13 9PL, UK

[2]Seismic Research Centre, University of the West Indies, St. Augustine, Trinidad and Tobago

[3]Montserrat Volcano Observatory, Flemmings, Montserrat

[4]Lunar and Planetary Laboratory, University of Arizona, Tucson, AZ 85721, USA

[5]Department of Mathematics and Centre for Nonlinear Dynamics, The University of Manchester, Manchester M13 9PL, UK

BE, 0000-0003-0069-0251; MB, 0000-0003-3779-4812; CH, 0000-0001-5734-0549; RC-A, 0000-0003-2713-5397; TC, 0000-0002-5968-5070; EPJ, 0000-0002-4836-8715; MV, 0000-0002-3794-5302; CJ, 0000-0003-2192-3616

*Correspondence: benjamin.esse@manchester.ac.uk

Abstract: Determining SO$_2$ emission time-series from explosive eruptions can provide important insights into the driving magmatic processes, however accurate measurements are difficult to collect. Satellite-based platforms provide SO$_2$ imagery, however translating this to the altitude- and time-resolved emission history required to unravel volcanic processes is a major challenge. This means SO$_2$ emission time-series are rarely quantified for major eruptions, producing a gap in our understanding of explosive volcanism.

Here, we combine SO$_2$ imagery collected by the TROPOspheric Monitoring Instrument (TROPOMI) with PlumeTraj, a back-trajectory analysis toolkit, to reconstruct the SO$_2$ emission prior to, and during, the explosive eruption of La Soufrière volcano, St Vincent, in April 2021. Precursory SO$_2$ emissions were quantified the day before the eruption, with emission rates in agreement with ground-based measurements. We estimate initial magma sulfur contents by comparing the measured SO$_2$ emissions with erupted magma volumes, finding that the initial explosion was sulfur poor (730 ppm S) compared to the main eruption phase (up to 3400 ppm S). This suggests that the initial explosion cleared old, previously degassed magma resident in the shallow plumbing system, followed by the eruption of the main, mostly un-degassed magma source.

Supplementary material: A supplementary figure showing the standard TROPOMI outputs for the days analysed is available at https://doi.org/10.6084/m9.figshare.c.6474314

Explosive volcanic eruptions are driven by the exsolution and expansion of volatile species during magma ascent, leading to fragmentation into volcanic ash and the formation of large eruption columns (Sparks and Wilson 1982). Explosive eruptions can be extremely dangerous, with pyroclastic density currents, ash fall and volcanic ballistics amongst the possible hazards. These pose a threat to life and can damage or destroy local critical infrastructure, including housing, transportation, electricity, and agriculture (Wilson *et al.* 2012). The energy imparted to the buoyant eruption column can allow explosive eruptions to inject reactive gases, aerosols and aerosol precursors into the upper troposphere and lower stratosphere. This greatly lengthens their residence time in the atmosphere from the order of a week to the order of a year (Karagulian *et al.* 2010) and increases their climate-altering potential (Robock 2000; Stothers 2009; von Glasow *et al.* 2009).

For these reasons, it is vitally important to correctly identify precursory signals and understand the driving processes for explosive volcanism to provide the best information to policy-makers and emergency organizations in the event of a major eruption (Sparks and Aspinall 2004). Volcanic gas measurements are a

key element in volcano monitoring strategies, as changes in the emission rate and composition of the emitted gases reflects the magma eruption rate and magma dynamics (Fischer *et al.* 1994; Duffell *et al.* 2003; Sparks 2003; Burton *et al.* 2007; Oppenheimer *et al.* 2011). Sulfur dioxide (SO_2) is the usual target species for gas emission rate quantification as it is typically the third most abundant gas in volcanic emissions (after CO_2 and H_2O) but has a negligible background atmospheric concentration (Symonds *et al.* 1994). Combined with absorption features at UV and IR wavelengths, this means that SO_2 is relatively easy to detect and quantify, making it a useful tracer for volcanic activity (Fischer *et al.* 1994; Burton *et al.* 2009; Platt *et al.* 2018; Salerno *et al.* 2018). Satellite remote sensing is particularly useful for volcano monitoring due to the wide (often global) spatial coverage of satellite instruments (Carn *et al.* 2016, 2017). This allows measurements of volcanoes without a dedicated ground-based gas-monitoring network, which is especially useful for remote or hard to access volcanoes.

Knowledge of the SO_2 emission rate time-series is critical in understanding the volcanic processes at play during an explosive eruption, but it is notoriously difficult to measure (Krotkov *et al.* 1997). Ground-based monitoring networks or traverse measurements are designed for passive degassing where the plume is preferably ash-free, at a relatively low altitude and advected into the ambient wind field. However, during explosive eruptions the plume is usually ash-rich and at a much higher altitude (sometimes reaching the stratosphere), often making accurate emission rate quantification from the ground impossible. Additionally, the hazards posed by an explosive eruption, for example from pyroclastic density currents, heavy ash fall or ejected volcanic ballistics, mean that monitoring networks can be damaged or destroyed, while manual ground-based measurements of gas emission rates can be too risky to conduct. Finally, most SO_2 monitoring networks utilize sunlight to quantify the emission rate, so measurements are restricted to daylight hours.

Because of the difficulties in quantifying gas emission rates from the ground during explosive activity, it is more common to use satellite imagery for major eruptions. Satellite-based instruments have a much lower spatial resolution than ground-based observations (typical pixel sizes of a few to tens of kilometres) and, depending on the orbit-type, have a lower temporal resolution (sub-hour to daily images). However, the coverage of such instruments is much greater, meaning it is easier to capture the entire eruptive plume. This means that the gas-loading from explosive eruptions is easier to quantify from satellite imagery than from the ground. Satellite observations of volcanic SO_2 have been available for several decades, with the Nimbus 7 Total Ozone Mapping Spectrometer (TOMS) detecting passive sulfur emissions from Ambrym volcano, Vanuatu in 1978 (Bani *et al.* 2009) and explosive SO_2 plumes from the 1982 eruption of El Chichón, Mexico (Krueger 1983). Several satellite instruments have been used to detect and quantify volcanic emissions (Carn *et al.* 2016), with the most recent advance delivered by the European Space Agency's (ESA) TROPOspheric Monitoring Instrument (TROPOMI) (Veefkind *et al.* 2012). This instrument provided an order of magnitude increase in the spatial resolution over the previous state-of-the-art one, the Ozone Monitoring Instrument (OMI) (Levelt *et al.* 2006), opening new frontiers in monitoring volcanic degassing from space (Theys *et al.* 2019). Although satellite SO_2 imagery provides useful information on the distribution of SO_2 in the atmosphere, it does not directly quantify the emission history of the volcano. This is especially the case for longer-duration eruptions, where a single satellite image may encompass multiple days' worth of emissions. For this reason, additional analysis is required to determine this essential information (Theys *et al.* 2013).

La Soufrière volcano (13.33° N, 34.18° W, summit elevation 1220 m a.s.l.) on the island of St Vincent has a long history of explosive volcanism (Cole *et al.* 2019). The most recent explosive eruption began on 9 April 2021 after just over three months of effusive lava dome growth, leading to a sequence of explosive eruptions that lasted until 22 April (Global Volcanism Project 2021). The eruption displaced over 16 000 people and caused widespread damage to houses and other infrastructure in the NW of the island, though a timely evacuation prevented casualties. Ash produced by the explosions fell on numerous islands in the region, including the Grenadines, Barbados, and Saint Lucia, leading to closures at the Argyle International Airport in St Vincent and the Grantley Adams International Airport in Barbados. The resulting eruption plumes mostly dispersed to the east over the Atlantic Ocean, where the emissions could be tracked for several days around the globe.

Here, we combine SO_2 imagery from TROPOMI with PlumeTraj, a back-trajectory analysis toolkit (Pardini *et al.* 2017, 2018; Queißer *et al.* 2019; Burton *et al.* 2021), to infer the SO_2 emission time-series of La Soufrière during the onset of the explosive activity (8–11 April 2021) and compare with eruption timings from Real-time Seismic Amplitude Measurement (RSAM) data available throughout the eruption. Although activity continued after this date, measurements of the SO_2 emissions were complicated as previously emitted SO_2 recirculated above the volcano and overprinted fresh emissions, making identification of newly erupted gas impossible with our method. We also combine erupted magma volumes from Sparks *et al.* (2023) with the

calculated SO$_2$ emission rates to determine the evolution of the initial magma sulfur content during this phase.

This paper demonstrates the ability of TROPOMI for near-real-time monitoring of ongoing eruptive processes as, although the analysis presented here has been applied after the event, the data required are available in near-real time and the analysis can be applied rapidly given sufficient computational power (the exact requirement varies with the extent and altitude of emissions). Therefore, the steps outlined here could be applied to a future volcanic eruption to provide timely, 24-hour SO$_2$ emission-rate measurements, supporting other real-time or near-real-time data streams, such as geophysical data or rapid geochemical analysis (e.g. Gansecki et al. 2019). We highlight that high temporal (sub daily) resolution gas emission time-series for strongly explosive eruptions have been reported only rarely (e.g. Moxnes et al. 2014; Pardini et al. 2018).

Data and methods

TROPOMI

TROPOMI is a hyperspectral imaging instrument and the sole payload of the ESA's Sentinel-5P satellite. Sentinel-5P is in a Sun-synchronous polar-orbit with a local (ascending) equatorial overpass time of 13:30. It launched on 13 October 2017, with scientific data available from May 2018. TROPOMI has a swath width of 2600 km, providing near-global daily coverage. The sensor is composed of four hyperspectral detectors covering wavelengths from the ultraviolet (UV; 270 nm) to the short-wave infrared (2385 nm) in eight bands (Veefkind et al. 2012). Retrievals of SO$_2$ are achieved using the UV and UV-visible spectrometers (specifically bands 2 and 3, covering 300–320 nm and 320–405 nm, respectively), which have a spatial resolution of up to 5.5 × 3.5 km at nadir (along-track × across-track, upgraded from 7.0 × 3.5 km from 6 August 2019) and a spectral resolution of 0.50–0.55 nm (Full Width Half Maximum) (Theys et al. 2019). The high spatial resolution of TROPOMI is a significant improvement over OMI, which had a spatial resolution of c. 24 × 13 km at nadir (de Graaf et al. 2016).

This study utilizes the offline Level 2 SO$_2$ data product (processor version 02.01.04), which is freely available through the ESA-Copernicus Sentinel-5P Pre-Operation Data-Hub (https://s5phub.coperni cus.eu). SO$_2$ slant column densities (SCDs) are retrieved using Differential Optical Absorption Spectroscopy (DOAS) using ground-reflected solar UV light as the light source (Platt and Stutz 2008; Theys et al. 2017). The SCD is then converted to a vertical column density (VCD) by dividing the SCD by a computed air mass factor (AMF) which combines geometrical and radiative transfer corrections (Palmer et al. 2001). However, knowledge of the SO$_2$ vertical profile is required to calculate the AMF, which is not known at the time of measurement. For this reason, four VCD values are calculated and reported, one for a polluted scene within the planetary boundary layer and three 1 km thick box profiles covering: 0–1 km above ground level, 6.5–7.5 km above sea-level and 14.5–15.5 km above sea-level. The box profiles are referred to as 1, 7 and 15 km VCDs in the TROPOMI documentation, which we will adopt from here onwards

One important factor for measurements of volcanic SO$_2$ plumes is the role of volcanic ash. The presence of volcanic ash in the plume can significantly degrade the retrieval process as it makes the plume optically thick; however, this process is not well understood. Andres and Schmid (2001) report that volcanic ash typically leads to an underestimation of SO$_2$ for UV correlation spectrometer (COSPEC) measurements, while Prata and Kerkmann (2007) raise the possibility of ash initially trapping SO$_2$, blocking it from view. Therefore, SO$_2$ retrievals in the presence of significant volcanic ash concentrations should be treated with caution.

PlumeTraj toolkit

The Level 2 SO$_2$ data product from TROPOMI captures the horizontal distribution of SO$_2$ in the atmosphere at the time of overpass. Reconstruction of an emission rate time-series from these data requires knowledge of the plume altitude at the time and location of measurement by the satellite, needed to accurately calculate the VCD, as well as the injection time and altitude from the volcano. There are several methods available to achieve this (Theys et al. 2013). Here we use a back-trajectory approach, known as PlumeTraj, to retrieve this vital information (Pardini et al. 2017, 2018; Queißer et al. 2019; Burton et al. 2021). The steps in this approach are outlined here and are displayed in Figure 1.

The raw SO$_2$ data from TROPOMI are first filtered for pixels with a VCD value above three times the reported random noise. These pixels are then filtered again, taking only those with at least two neighbouring pixels that also pass the noise threshold. This is done to select plume pixels while ignoring lone pixels that happen to be above the noise threshold.

The filtered pixels are then taken forward for the back-trajectory analysis. All trajectories are calculated with the Hybrid Single-Particle Lagrangian Integrated Trajectory (HYSPLIT) dispersal model (Stein et al. 2015) using the National Oceanic and Atmospheric Administration (NOAA) Global Forecast System (GFS) 0.25° global meteorological
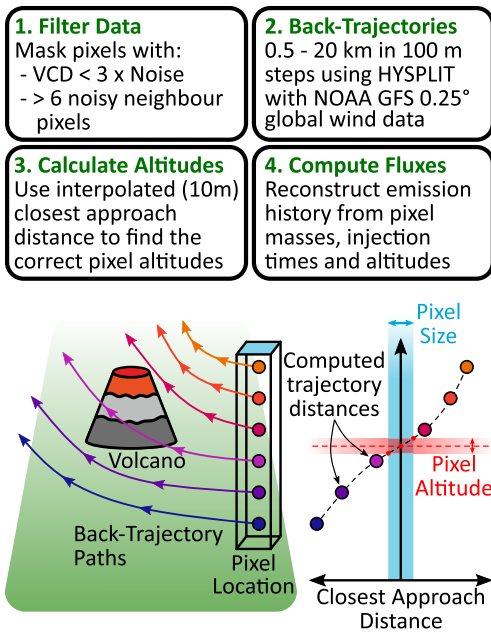
Fig. 1. Overview of the PlumeTraj methodology, outlining the main steps in the back-trajectory analysis.

data from the National Centers for Environmental Prediction (NCEP, available from https://www.ready.noaa.gov/archives.php). The GFS data used have a temporal resolution of 1 hour and have 55 vertical pressure layers (https://www.ready.noaa.gov/data/archives/gfs0p25/readme_gfs0p25_info.txt, accessed 12 June 2022). HYSPLIT has a model output timestep of 10 minutes and interpolates the GFS meteorological data down to the requested time and position for each trajectory step. For each pixel, back-trajectories are launched at multiple altitudes from the TROPOMI pixel centre position. The exact altitude grid used depends on the application; in this case altitudes from 0.5–20 km a.s.l. were used at a spacing of 0.1 km. The trajectories are calculated 24 hours back in time under most circumstances

Due to wind shear in the atmosphere, the wind direction at a given location will vary with altitude. This means that trajectories initialized from the pixel location will follow different paths depending on the altitude at which they start. If the trajectories for a pixel return to the target volcano, the closest approach distance of each trajectory to the vent will vary as a function of altitude due to the different paths they take. For a given pixel, a 'signed' closest approach distance is calculated as a function of trajectory initialization altitude, where the sign is negative to the left of the volcano and positive to the right. Here, left and right are defined with respect to the

pixel–volcano vector. The correct plume altitude can then be found by calculating the trajectory initialization altitude at which a trajectory would pass directly over the volcano. A level of uncertainty is introduced into this as the pixels have a finite size, therefore an uncertainty range in altitude is calculated by considering the range of altitudes around the retrieved pixel altitude that have trajectories that pass within a pixel's width of the volcano. The plume altitude and uncertainty bounds are calculated by a linear interpolation between the calculated trajectories.

Once the plume altitude has been computed, three final trajectories are calculated for each pixel, initialized at the retrieved altitude and the upper and lower limits calculated from the pixel size. These trajectories provide the final injection altitude and time of each pixel, as well as an associated uncertainty from the pixel size. Note that the trajectories are re-calculated rather than using the interpolated values from the initial run to ensure no artefacts were introduced by the interpolation. The calculated plume altitude (at the point of measurement) is used to determine the true VCD by linearly interpolating between the pre-calculated box VCDs, which is then converted to a mass by multiplying by the pixel area. The uncertainty in plume altitude is combined with the precision and trueness values provided in the TROPOMI L2 SO_2 data, representing the random and systematic uncertainties on the VCD respectively, to produce an overall uncertainty on the corrected pixel VCD and mass. Note that this method requires that a single injection time and altitude are valid for a single pixel. This assumption is no longer valid if earlier emissions are recirculated back to the volcano by local weather patterns. For the results presented in this paper, it is not possible to separate the old and fresh emissions contained within a single pixel after 12 April and so PlumeTraj cannot be applied from this date.

The individual pixel data are then combined to produce the emission history up to the time of overpass. Firstly, a two-dimensional grid is generated, with injection time on the x-axis and injection altitude on the y-axis. The mass contributions (using the plume altitude corrected VCDs) from each pixel are summed on this grid, with the mass from each pixel distributed in an asymmetrical two-dimensional Gaussian function (in time and altitude). The distribution is centred on the calculated injection time and altitude, with sigma values computed from the upper- and lower-plume altitude trajectories. This provides an SO_2 emission rate distribution, which can be integrated over all altitudes to provide the emission rate time-series. In this way, the emission history of an eruption can be reconstructed from the two-dimensional static SO_2 imagery measured by TROPOMI.

In practice, there are often multiple altitudes at which a back-trajectory intersects the vent due to inversions in wind direction in the atmosphere, each corresponding to a different injection altitude and time. This is particularly true for larger eruptions where the plume could be injected over a wide range of altitudes throughout the troposphere and lower stratosphere. It is not possible to distinguish between the different solutions without additional information, such as the timing of a particular event (from seismic data or visual observations for example) or from an independent measure of the injection altitude (such as from radar or visual estimates). In this case, solutions were selected using timings and plume altitude estimations taken from seismic data and reports from the Global Volcanism Program (GVP), which incorporates reports from the National Emergency Management Organisation (NEMO) of the Government of Saint Vincent and the Grenadines and the University of the West Indies Seismic Research Centre (UWI-SRC) (Global Volcanism Project 2021). We note that such observations likely report the altitude of the visible ash plume and not specifically the SO₂. This may lead to the incorrect altitude if these are not collocated and so care should be taken when using these observations.

It is also possible to use a combined forward/backward trajectory technique to constrain the correct altitude, as outlined by Pardini *et al.* (2018). In this method, forward trajectories are launched from the point of measurement at multiple altitudes and the resulting position compared to observations of the plume position the next day. This method was not applied in this case as, although the plumes were visible the next day, the emissions were roughly continuous and so it was not possible to distinguish which section of the plume corresponded to the observations from the previous day.

Magma sulfur contents

By combining the emission rates calculated by PlumeTraj with estimates of eruption volumes, it is possible to make inferences of the original magma sulfur content.

$$S_{content} = \frac{M_{SO_2} \cdot 0.5}{M_{magma}} \times 10^6 \qquad (1)$$

where $S_{content}$ is the sulfur content (ppm), M_{SO_2} is the measured SO₂ mass (kg), 0.5 is the mass ratio of sulfur in SO₂ and M_{magma} is the measured mass of magma erupted (kg). We use individual explosion volumes calculated from the seismic signals detected during the eruption from Sparks *et al.* (2023) to calculate the erupted magma masses.
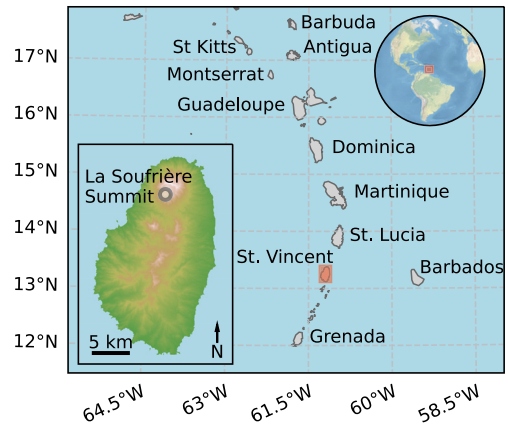

Fig. 2. Map showing the location of La Soufrière and St Vincent. Top right inset map shows the location of the Lesser Antilles Arc in the world and the bottom left inset map shows a zoomed view of St Vincent, coloured by elevation. Source: elevation data are from the Shuttle Radar Topography Mission (SRTM) Elevation Dataset (NASA 2002).

Overview of La Soufrière volcano

Geological setting and past activity

La Soufrière is situated in the north of the island of St Vincent, the largest island of the St Vincent and the Grenadines archipelago, in the southern part of the Lesser Antilles Island Arc, a roughly 800 km long chain of islands bounding the Caribbean Sea (Fig. 2). Volcanism along the arc stems from the westward subduction of the North American plate under the Caribbean plate (Fedele *et al.* 2021). Several of the islands in the Lesser Antilles Arc have active volcanoes that have had historical eruptions, including Soufrière Hills Volcano on Montserrat, La Soufrière on Guadeloupe, and Mount Pelée on Martinique. Before the explosive 2021 eruption of La Soufrière, St Vincent, the most recent subaerial eruption in the region was that of Soufrière Hills Volcano, Montserrat, which last erupted in 2010, with ongoing activity to the present.

The island of St Vincent is built from the remains of previous volcanic centres, with the ages of previous centres increasing towards the south (Briden *et al.* 1979). La Soufrière is the current active centre and is one of the most active volcanoes in the Lesser Antilles Arc. It has had at least six explosive eruptions in the last 1000 years, including two undocumented prehistoric eruptions and four that occurred in historical times, dated to 1440 CE, 1580 CE, 1718 CE, 1812 CE, 1902 CE and 1979 CE (Cole *et al.* 2019). Deposits from these eruptions can be found on St Vincent and the surrounding islands.

Some of these eruptions resulted in casualties, with the 1902 eruption claiming over 1500 lives (Pyle *et al.* 2018). Several effusive eruptions have also occurred, including in 1971–72 (Aspinall *et al.* 1973) and the growth of a lava dome after the explosive phase of the 1979 eruption, while the undocumented eruptions before 1718 may have included dome-building activity. The dome from the 1979 eruption was present until the onset of explosive activity in April 2021.

2021 eruption timeline

The timeline of activity on St Vincent is summarized here from a bulletin report from the Global Volcanism Program, Smithsonian Institute (Global Volcanism Project 2021). This report collated information from bulletins, press releases and reports from UWI-SRC, NEMO and other observations on the eruption. An overview of the eruption response is also available in Joseph *et al.* (2022).

The activity at La Soufrière began with an effusive, dome-building eruption, first identified on 27 December 2020, with visual confirmation on 29 December from personnel from NEMO. This led to the deployment of UWI-SRC scientists and technicians from Trinidad on 31 December to monitor the ongoing activity. Over the next few months, the volcano was carefully observed, and the monitoring network strengthened. Gas and steam emissions were observed from the dome, with SO_2 first detected on 1 February 2021 by MultiGAS measurements. During this time the lava dome grew steadily at a rate of roughly 1.8 $m^3 s^{-1}$ (Dualeh *et al.* 2023), with a final measured size on 19 March of 105 m tall, 921 m long and 243 m wide, and a total estimated volume of $13.13 \times 10^6 m^3$. Earthquake swarms were detected during 23–24 March and on 5–6 April, attributed to magma movement under the lava dome.

Episodes of tremor began on 8 April 2021 at 07:00 (all times given in UTC, AST+ 4 hours), slowly increasing through the day. Gas and steam emissions from the dome were visible, with SO_2 detectable by DOAS during an offshore traverse off the west coast for the first time. The first detections of SO_2 from space (by TROPOMI) were also recorded that day. This escalation in activity prompted a raise in the Alert Level to Red (the highest level) and evacuations were ordered for the northern area of the island. The rate of lava extrusion of the new lava dome was also observed to dramatically increase to roughly 17.5 $m^3 s^{-1}$ in the two days before the transition to explosive activity (Dualeh *et al.* 2023).

The explosive eruption of La Soufrière began on 9 April 2021. Scientists monitoring the activity from the Belmont Observatory in the southern region of St Vincent reported an explosion at 12:40, which produced an ash plume that drifted ENE. This was followed by another period of ash-venting beginning at roughly 18:00, initially rising to 4 km but building to 16 km and lasting several hours. A third venting period began at 22:35, continuing overnight and into the next day with a phase of continuous explosions. Into 11 April, the style of activity shifted to more discrete explosions with the spacing between explosions increasing. Over the following days, the explosive activity continued to decrease in intensity and the period between explosive episodes increased, with the final explosions taking place on 22 April at around 15:08.

After the onset of the explosive activity, SO_2 emission rate measurements were performed by boat from the west coast, reporting SO_2 emission rates of 2.7–12.0 $kg s^{-1}$ between 14 April and 3 May. TROPOMI continued to measure substantial SO_2 VCDs above and around La Soufrière, as shown in Figure 3; however, much of this appears to be previously emitted gas returned to the volcano. This means that identifying newly erupted SO_2 after 11 April is very difficult. Since the last explosive episode on 22 April, there has been no detectable SO_2 from La Soufrière by TROPOMI and activity at the volcano remains low.

Results

Back-trajectory analysis

PlumeTraj was applied to TROPOMI SO_2 imagery on four days, covering 8–11 April 2021. Figure 4 shows the corrected SO_2 VCD, plume age at the time of overpass and plume altitude for the successful pixels for each day, as well as the raw UV aerosol index (UVAI) for each day reported by TROPOMI. The UVAI is used to determine the presence of UV-absorbing aerosols in the atmosphere, including volcanic ash, which present themselves as a positive value (Carn and Krotkov 2016). This is a useful, semi-qualitative flag for the presence of volcanic ash (or other UV-absorbing aerosol). In this case the 340/380 nm UVAI is used. Note that 24-hour back-trajectories were used for 8–9 April, 36-hour back-trajectories for 10 April and 48-hour back-trajectories for 11 April. The longer length trajectories were primarily used to exclude emissions from the previous day in the results, as shown by the extensive region of the plume that is older than 24 hours on 11 April (Fig. 4n).

The pixel results were then used to reconstruct the emission history up to the time of overpass for each day. This is shown in Figure 5, alongside the RSAM time-series, collected by UWI-SRC, for comparison. An overview of the average and peak SO_2 emissions
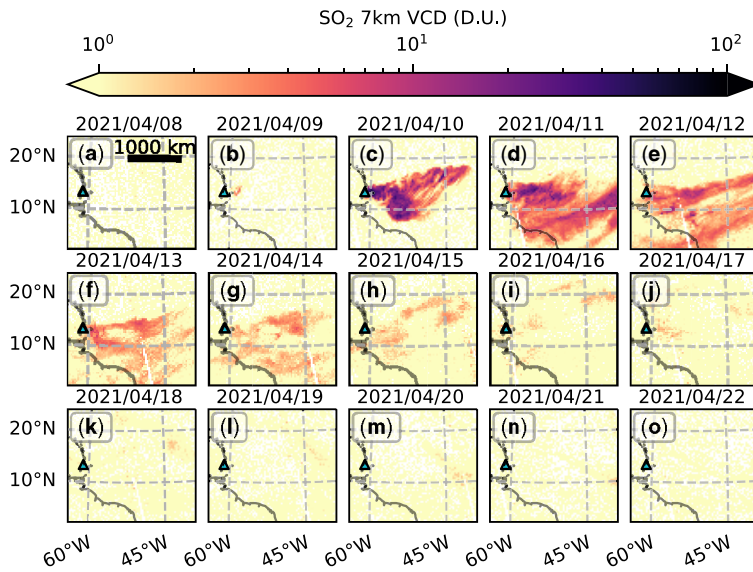
SO₂ emissions from 2021 La Soufrière eruption

Fig. 3. Overview of the SO₂ distributions measured by TROPOMI 8–23 April 2021 around La Soufrière (light blue triangle). The product displayed is the raw 7 km VCD (log scale) reported in the Level 2 operational output data from TROPOMI. Note that the SO₂ plume was transported much further than shown here, with emissions detected around the globe. Multiple orbits are shown for each day, each separated in time by approximately 1 hour and 40 minutes per orbit.

and injection altitudes for each day are shown in Table 1.

The precursory degassing detected on 8 April can be seen heading towards the NW, with no evidence of ash emission (Fig. 4a–d). The total mass of SO_2 measured is 31 (± 21) $\times 10^3$ kg. A general increase in the observed emission rate can be seen throughout the day up to 12:00, before dropping in the 6 hours prior to the overpass (Fig. 5b).

The emission rates are small, reaching a maximum of only 1.4 (± 1.0) kg s^{-1}, likely on the edge of the detection limit for TROPOMI. DOAS traverse measurements on this day also detected SO_2 for the first time, measuring an emission rate of 0.93 (± 0.07) kg s^{-1} (Joseph *et al.* 2022), in good agreement with the results from TROPOMI. The injection altitude (2.5–4 km) is significantly higher than the volcano summit (1.22 km). Comparing with the RSAM time-series shows a roughly coincident onset, with the RSAM rising sharply then dying away as the SO_2 emission rate increases (Fig. 5c).

The overpass on 9 April captured the initial explosion nicely as it drifted eastward (Fig. 4e–h). A small, early and low altitude emission is visible towards the NW, likely a continuation of the precursory degassing detected on 8 April. The main explosive plume was emitted in a short time frame (2–3 hours) at roughly 13–15 km altitude (Fig. 5d). There is evidence of some ash in the main core of the plume as shown by the positive UVAI values (Fig. 4h), though

the maximum UVAI values are not spatially aligned with the maxima in the observed SO₂.

The total calculated mass of SO_2 for the orbit on 9 April is 1.9 (± 0.6) $\times 10^6$ kg, with a peak emission rate of 330 (± 100) kg s^{-1}. The peak in SO_2 emission correlates well with the spike in RSAM (Fig. 5f), though the duration of SO_2 emissions is longer. The RSAM can be seen to increase into the evening with the onset of the phase of continuous explosions, however this occurred after the overpass time and so was not captured on this day.

The next overpass on 10 April captured the emissions from the phase of continuous sub-Plinian activity overnight on 9/10 April (Fig. 4i–l). Much higher concentrations of SO_2 were observed in this overpass than the previous days and there is a strong ash signal in the UVAI (although this diminishes rapidly with distance from the vent).

The reconstructed emission time-series shows continuous emission of SO_2 throughout the day, primarily at an altitude of roughly 14 km (Fig. 5g). The emission rate is not steady with time, building to a maximum of 6500 (± 2000) kg s^{-1} at roughly 21:45 on 9 April during the continuous phase, before dropping (Fig. 5h). A second peak is seen at roughly 13:00 on 10 April after the transition to discrete explosions (Fig. 5i). There is a sharp decrease in emission rate roughly four hours prior to the time of overpass, most likely due to the higher concentration of ash in the younger plume near the vent impacting
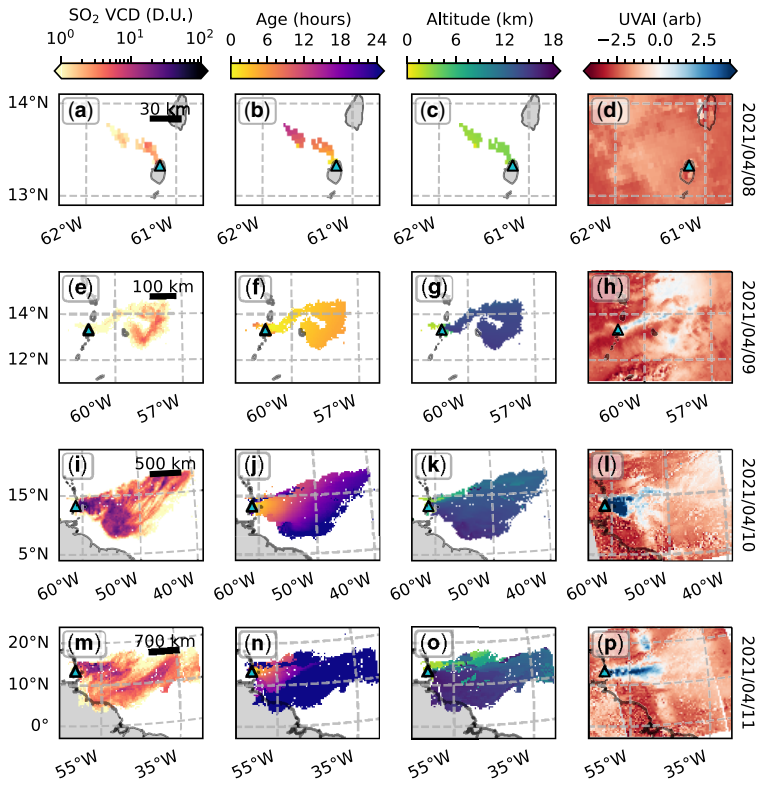
Fig. 4. Results of the PlumeTraj analysis for 8–11 April 2021, showing corrected SO_2 VCD (**a, e, i, m**, log scale), plume age at the time of overpass (**b, f, j, n**) and plume altitude (**c, g, k, o**), as well as the raw UV aerosol index for the scene (**d, h, l, p**). The location of La Soufrière is given by the light blue triangle.

the SO_2 retrieval (Fig. 4l). The total mass of SO_2 measured for this orbit is 310 (± 90) $\times 10^6$ kg.

The explosive activity continued into 11 April, as seen in the next day's overpasses (Fig. 4m–p). Note that here the plume is stretched across three separate orbits, each measured roughly 1 hour and 40 minutes apart, though the bulk of the plume is in the central orbit. There should be no problem of double counting emissions in separate orbits as the plume is moving eastwards while TROPOMI moves westwards with increasing orbit number.

Much of the SO_2 was again emitted at roughly 15 km, although with a wider spread of altitudes (Fig. 5j). The timings of the discrete explosions can be seen in the RSAM time-series (Fig. 5l), with an increase in SO_2 emission rate seen after several (Fig. 5k), though the correlation is not perfect. As on 10 April, a drop in the measured emission rate is seen prior to the overpass times.

As already highlighted, much of the SO_2 in the frame was emitted over 24 hours prior to the overpass time, so simply summing the visible SO_2 mass would lead to a significant overestimation

due to double counting of older emissions. Using the plume ages calculated by PlumeTraj, the mass emitted in the 24 hours before the first of the three overpasses was isolated and calculated to be 140 (± 40) $\times 10^6$ kg, roughly half that of the previous day.

TROPOMI continued to observe significant concentrations of SO_2 around La Soufrière for several days. Much of this was previously emitted SO_2 that was returned to the volcano; however, emissions from explosions on the 14 and 22 April are visible. While other explosions did occur during this time, either the timings of the events were not viable for TROPOMI, or the emissions were not visible under the signal of recirculated SO_2.

It is worth highlighting the importance of knowing the plume altitude for determining the mass of SO_2 in each pixel. The difference between the 1 km and 15 km VCDs can be greater than an order of magnitude, demonstrating that knowing the correct plume altitude is key in determining the correct SO_2 mass and emission rates. Supplementary Figure S1 shows the standard 1, 7 and 15 km box
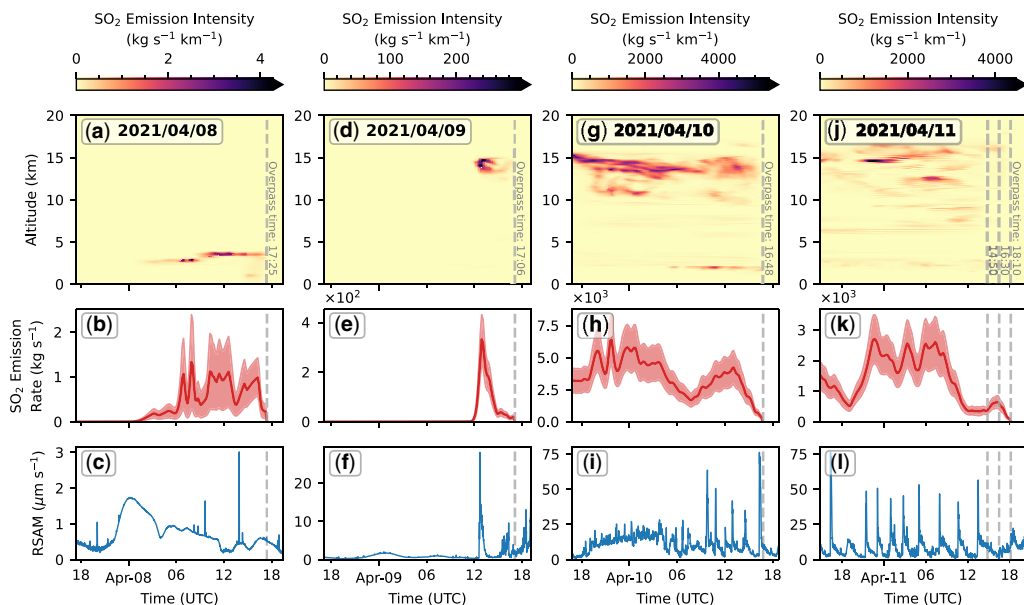
Fig. 5. Reconstructed SO$_2$ emissions for 8 (**a**, **b**, **c**), 9 (**d**, **e**, **f**), 10 (**g**, **h**, **i**) and 11 (**j**, **k**, **l**) April 2021. The top row shows the SO$_2$ emission intensity, a measure of the emission of SO$_2$ as a function of time and altitude. The resolution of the time grid is 10 minutes, and the resolution of the altitude grid is 100 m. The middle row shows the integrated SO$_2$ emission rate time-series, with the shaded region giving the uncertainty estimate. The bottom row shows the RSAM time-series. Dashed vertical lines give the overpass times for each day, with three orbits and associated overpass times on 11 April. Note different scales are used each day.

VCDs available from the TROPOMI L2 SO$_2$ product, as well as the corrected VCDs from the Plume-Traj analysis for each day analysed here.

Magma sulfur content

Original magma sulfur contents were calculated for 9, 10 and 11 April using the average SO$_2$ emission rates in given time windows (Table 2). Note that this was not applied on 8 April as these were effusive emissions. Magma masses were calculated by summing the volume estimates from Sparks *et al.* (2023) for the individual events taking place within

these time windows and multiplying by a Dense Rock Equivalent (DRE) density of 2750 kg m^{-3}.

Seismic records indicate that the duration of the initial explosion on 9 April was 14.6 minutes (Sparks *et al.* 2023), which is much shorter than the duration of SO$_2$ emissions seen by PlumeTraj. This likely reflects uncertainties in the back-trajectories, as well as smoothing effects introduced by the plume ascent process and umbrella cloud (Woodhouse *et al.* 2016). This means that our measured SO$_2$ emission rates are likely underestimates, therefore for this event we use the total SO$_2$ measured in the plume to calculate the S content with equation (1). For the 10 and 11 April, it is not possible to resolve individual

Table 1. *Daily measured mean and peak measured SO$_2$ emission rates and injection altitudes*

Overpass time (UTC)	Injection altitude (km)	Mean emission rate (kg s^{-1})	Peak emission rate (kg s^{-1})
8 April 2021 17:25	3.5 ($\pm$1.0)	0.7 ($\pm$0.5)	1.4 ($\pm$1.0)
9 April 2021 17:06	14.7 ($\pm$1.0)	220 ($\pm$70)	330 ($\pm$100)
10 April 2021 16:48	13.7 ($\pm$1.0)	3800 ($\pm$1200)	6500 ($\pm$2000)
11 April 2021 14:50, 16:30 and 18:10	14.8 ($\pm$2.3)	1700 ($\pm$500)	2700 ($\pm$800)

Average emission rates were calculated using the following windows: 2021/04/08 06:00–2021/04/08 340 17.20, 2021/04/09 12:30–2021/04/09 14:20, 2021/04/09 17:00–2021/04/10 13:10, 2021/04/10 18:00–2021/04/11 08:30 for 8, 9, 10 and 11 April, respectively. Uncertainty on injection altitude was 342 estimated from spread in total injected mass around the modal altitude (see supporting datasets).

Table 2. *Calculation of original magma sulfur content for explosive activity*

Period start	Period end	Number of explosions	Magma volume (km^3)	Magma mass (Mt)	SO$_2$ Emission rate (kg s^{-1})	Total SO$_2$ mass (kt)	S content (ppm)
9 April 12:30	9 April 14:20	1	0.5 ($\pm$0.2)	1.3 ($\pm$0.5)	220 ($\pm$70)	1.9 ($\pm$0.6)	730 ($\pm$230)
9 April 17:00	10 April 13:10	17	15 ($\pm$6)	41 ($\pm$16)	3800 ($\pm$1200)	290 ($\pm$90)	3400 ($\pm$1100)
10 April 18:00	11 April 08:30	7	11 ($\pm$4)	29 ($\pm$11)	1700 ($\pm$500)	90 ($\pm$30)	1500 ($\pm$500)

The number of explosions and erupted magma volumes for each period are taken from Sparks *et al.* (2023, table 3) and converted to masses assuming a density of 2750 kg m^{-3}. SO$_2$ masses are calculated by multiplying the mean emission rate by the duration of the period, except for the 9 April where the total SO$_2$ in the plume is used.

explosions, so the mean SO$_2$ emission rate in the given time windows is used to generate a total SO$_2$ mass for that window, which is then combined with the magma mass to calculate the S content. The windows for the averaging periods were manually selected from 24 hours before the latest overpass and to avoid the impact of ash on 10 and 11 April.

These results show that the initial explosion was significantly poorer in sulfur than the following activity. The sulfur content measured on the 11 April is lower than on 10 April, although this could be due to the more extensive ash plume visible on this day (Fig. 4p) leading to an underestimate in SO$_2$ mass due to either uptake on ash particles or attenuation of the light passing through the plume resulting in greater than usual light dilution impacts (Varnam *et al.* 2020).

Discussion

During the effusive degassing phase of the eruption, SO$_2$ was not measurable from the operational SO$_2$ product of TROPOMI except on 8 April, the day before the onset of explosive activity. This precursory emission on 8 April was injected at 3–4 km altitude, several kilometres above the 1220 m summit. The emission rates were low, peaking at only 1.4 ($\pm$0.8) kg s^{-1}, within uncertainty of the value of 0.93 ($\pm$0.07) kg s^{-1} from a DOAS traverse measurement taken that day.

SO$_2$ emission time-series were also reconstructed for the first three days of explosive activity (9–11 April). The initial explosion on 9 April had a peak SO$_2$ emission rate of 330 ($\pm$100) kg s^{-1} and a total emitted mass of SO$_2$ of 1.9 ($\pm$0.6) $\times$ 10^6 kg. Although some evidence of ash was detected in the plume, the UVAI values are relatively low (compared to the following activity) and so it is assumed to not impact the SO$_2$ retrieval significantly. This initial explosion was followed that evening by a phase of continuous explosions that were richer in sulfur.

The peak emission rate during this phase was 6500 ($\pm$2000) kg s^{-1} in the evening of 9 April, approximately 20 times that of the initial explosion. The injection altitude of the SO$_2$ was roughly 13–15 km throughout. Over the next days, the frequency of explosions dropped but the emission rate remained high, between 1000 and 2700 kg s^{-1} on 11 April. Data from both 10 and 11 April show a strong decrease in the measured emission rate in the hours before the satellite overpass, suggesting that the presence of ash in the proximal plume is strongly impacting the retrieved emission rate before it settles out down wind. After 11 April the SO$_2$ emissions were not as clear due to recirculated SO$_2$ from previous activity overprinting the fresh emissions, so emission rates could no longer be determined as individual pixels would have multiple injection times associated to different portions of the total SO$_2$ column.

One of the major benefits of using PlumeTraj is the ability to discriminate between fresh and older emissions, as demonstrated by the measurements on 11 April. Here, much of the visible plume was older than 24 hours and so had been measured already the previous day. If the total pixel masses in the orbit are simply summed, this will lead to significant double counting of emissions from the previous day. However, with PlumeTraj it is possible to isolate the emissions from the 24-hour time window prior to the overpass. In this case we determine that 140 ($\pm$40) $\times$ 10^6 kg had been emitted in the 24 hours prior to the overpass on 11 April (calculated by summing the masses of all pixels that were emitted in this time frame). This is approximately a third of the 410 ($\pm$130) $\times$ 10^6 kg of total visible SO$_2$ emissions in the region analysed, which itself does not include the entirety of the SO$_2$ plume on this day.

Pre-eruptive magma sulfur contents were calculated for 9, 10 and 11 April using the reconstructed SO$_2$ emission rates and injection altitudes (Table 2). These results show that the initial explosion on 9 April was significantly poorer in sulfur compared to the following activity.

From these results, we propose the following eruption mechanism. The main magma body driving the eruption first caused the extrusion of a new lava dome around the 1979 dome already present. This new dome consisted of old, already degassed magma left by the previous activity, hence why negligible SO_2 was detected during this phase. The SO_2 degassing from the fresh magma source was trapped within the plumbing system, causing the pressure within to build with time. Eventually this reached a critical level, forcing its way out as the degassing visible the day before the explosive activity and eventually driving the initial explosion. This ejected the previously degassed magma within the system and cleared the way for the eruption of the fresh, SO_2-rich magma in the main phase of the eruption five hours later.

It is worth noting that the emission calculations assume that the measured SO_2 represents the total emitted sulfur from the magma. This could be incorrect as, firstly, SO_2 can be converted to H_2SO_4 after emission and, secondly, SO_2 is not the only sulfur species emitted by volcanic eruptions. The former is not likely to be significant here as typical e-folding times for conversion of SO_2 in stratospheric plumes is several days (Karagulian *et al.* 2010) and the measurements presented here only consider emissions less than 24 hours old. The latter is more difficult to address.

Volcanic sulfur emissions are dominated by SO_2 and H_2S (Oppenheimer *et al.* 2011) and, though SO_2 is readily measured by both UV and IR satellite instruments, reports of H_2S are few and limited to IR instruments (Clarisse *et al.* 2011; Sigmarsson *et al.* 2013). The sulfur speciation of volcanic plumes depends on the temperature, pressure and oxidation state of the magma (Aiuppa *et al.* 2005) as well as post-eruptive chemical processes, especially within the hot core of volcanic plumes (Hoshyaripour *et al.* 2012). These studies suggest that, although H_2S is likely a significant portion of the sulfur budget for divergent plate and hot spot volcanoes, SO_2 is generally dominant for convergent plate volcanism, as with La Soufrière. Nonetheless, the sulfur speciation is a key source of uncertainty in estimating sulfur emissions, highlighting the further work needed on constraining H_2S abundances within volcanic plumes.

Finally, it is interesting to compare the gas emissions of La Soufrière with SO_2 emission rates measured during another major eruption quantified with PlumeTraj: the 2015 eruption of Calbuco in Chile. Pardini *et al.* (2018) reported two average emission rates for the two impulsive explosive phases of this eruption. Phase 1 lasted roughly 2 hours and produced an average SO_2 emission rate of 25 000 kg s^{-1}, while phase 2 lasted roughly 6 hours with an average emission rate of 7200 kg s^{-1}.

The much higher emission rate in phase 1 of this eruption compared with St Vincent in 2021 reflect both a higher mass eruption rate and injection altitude (17 km for Calbuco v. 14 km for St Vincent) but also the presence of pre-existing accumulated gas in the magmatic system of Calbuco, which was preferentially erupted in the first phase. This highlights the dramatically different eruption dynamics of the two eruptions, with Calbuco having a gas-rich initial explosive phase produced by the long-term evolution of the magma in a crustal reservoir, whereas St Vincent shows an initial clearing phase followed by what appears to be a syn-eruptive gas exsolution process with no indication of pre-existing gas.

Conclusions

The eruption of La Soufrière, St Vincent, from 9–22 April was the largest explosive emission of SO_2 from the Caribbean in the satellite era and one of the largest eruptions globally in recent years. Daily measurements of atmospheric SO_2 from TROPOMI were analysed during the explosive eruption, as well as for the effusive activity in the months before. Although SO_2 was reported from MultiGAS measurements on 1st February, it remained below the detection limit for both ground- and satellite-based remote sensing methods during the effusive phase of the eruption until the day before the onset of explosive activity. The explosive phase began with an SO_2-poor, vulcanian explosion at 12:40 on 9 April, followed by a phase of continuous sub-Plinian explosions approximately 5 hours later. This continued overnight, transitioning into discrete explosions that decreased in intensity and frequency over the following days. The final explosion took place on 22 April and there has been no significant activity since.

By combining daily TROPOMI SO_2 imagery with PlumeTraj we were able to reconstruct the time- and altitude-resolved SO_2 emissions over the first three days of the eruption. We also calculated pre-eruptive magma sulfur contents by combining the emitted SO_2 mass with calculated erupted magma volumes. These results indicate that the lava dome extruded during the effusive phase of the eruption consisted of previously degassed magma from the prior activity in 1979. SO_2 exsolved from the fresh magma was trapped within the plumbing system until the pressure was sufficient to drive the initial explosion. This explosion ejected this older magma from the conduit, clearing the way for the eruption of the fresh, SO_2-rich magma in the main phase of the eruption.

Although PlumeTraj is a powerful tool for unravelling the emission history of volcanic eruptions,

there are several current limitations to this method. Firstly, as already discussed, there can be several altitudes that successfully return to the volcano, so we must rely on additional observations of the eruption to determine the correct solution, which are not always available. This could be mitigated by incorporating spectral plume altitude estimations as the pixel-by-pixel a priori estimate (Hedelt *et al.* 2019; Theys *et al.* 2022). Secondly, the trajectories used do not consider any plume spreading caused by the umbrella cloud of the eruption, which is likely the cause of the artefacts at the edges of the plume on 10 and 11 April. Addressing this issue requires incorporating an additional spreading factor and is ongoing work. Thirdly, PlumeTraj is not able to determine SO_2 emission rates when the SO_2 recirculates back to the volcano and overprints fresh emissions, as was seen after 11 April. There is no way to determine how much of the SO_2 seen in the pixel is fresh or old, so the emission rate cannot be determined. Finally, for volcanic cases the presence of significant loadings of volcanic ash in the plume can be seen to degrade the SO_2 retrieval, leading to an underestimate in the emission rate. Resolving this issue is not currently possible and would require knowledge of the atmospheric ash loading and the ash particle optical properties, so the best option currently is to avoid very ash-rich regions of the plume.

This paper demonstrates how satellite imagery combined with back-trajectory analysis can provide insights into eruptive processes, filling a current gap in our understanding of explosive volcanism. Although in this case the analysis was applied after the event, the required TROPOMI and wind field data are publicly available in near-real time and, while the required computational processing power is not trivial, it is possible to perform on a timescale of hours given sufficient computational resources. This opens the possibility of producing 24-hour SO_2 emission rate measurements in near-real time during volcanic eruptions, providing crisis managers with vital information on the eruptive processes during an ongoing crisis. This information could be used to better understand the ongoing volcanic activity and help mitigate the risks posed by future eruptions.

Author contributions **BE**: data curation (lead), investigation (lead), methodology (lead), software (equal), visualization (lead), writing – original draft (lead), writing – review & editing (equal); **MB**: conceptualization (supporting), funding acquisition (lead), methodology (supporting), project administration (lead), supervision (lead), writing – review & editing (equal); **CH**: conceptualization (supporting), methodology (supporting), software (equal), writing – review & editing (equal); **RC-A**: conceptualization (supporting), investigation (supporting), writing – review & editing (equal); **TC**: conceptualization (supporting), writing – review & editing (equal); **EPJ**: conceptualization (supporting), writing – review & editing (equal); **MV**: conceptualization (supporting), software (equal), writing – review & editing (equal); **CJ**: conceptualization (supporting), writing – review & editing (equal).

References

Aiuppa, A., Inguaggiato, S. *et al.* 2005. H_2S fluxes from Mt. Etna, Stromboli, and Vulcano (Italy) and implications for the sulfur budget at volcanoes. *Geochimica et Cosmochimica Acta*, **69**, 1861–1871, https://doi.org/10. 1016/j.gca.2004.09.018

Andres, R.J. and Schmid, J.W. 2001. The effects of volcanic ash on COSPEC measurements. *Journal of Volcanology and Geothermal Research*, **108**, 237–244, https://doi.org/10.1016/S0377-0273(00)00288-2

Aspinall, W.P., Sigurdsson, H. and Shepherd, J.B. 1973. Eruption of Soufrière Volcano on St. Vincent Island, 1971–1972. *Science (New York, NY)*, **181**, 117–124, https://doi.org/10.1126/science.181.4095.117

Bani, P., Oppenheimer, C. *et al.* 2009. Surge in sulphur and halogen degassing from Ambrym volcano, Vanuatu. *Bulletin of Volcanology*, **71**, 1159–1168, https://doi. org/10.1007/s00445-009-0293-7

Briden, J.C., Rex, D.C., Faller, A.M. and Tomblin, J.F. 1979. K–Ar geochronology and palaeomagnetism of volcanic rocks in the Lesser Antilles island arc. *Philosophical Transactions of the Royal Society of London Series A, Mathematical and Physical Sciences*, **291**, 485–528, https://doi.org/10.1098/rsta.1979.0040

SO₂ emissions from 2021 La Soufrière eruption

Burton, M., Allard, P., Muré, F. and La Spina, A. 2007. Magmatic gas composition reveals the source depth of slug-driven strombolian explosive activity. *Science (New York, NY)*, **317**, 227–230, https://doi.org/10.1126/science.1141900

Burton, M.R., Caltabiano, T., Murè, F., Salerno, G. and Randazzo, D. 2009. SO₂ flux from Stromboli during the 2007 eruption: results from the FLAME network and traverse measurements. *Journal of Volcanology and Geothermal Research*, **182**, 214–220, https://doi.org/10.1016/j.jvolgeores.2008.11.025

Burton, M., Hayer, C., Miller, C. and Christenson, B. 2021. Insights into the 9 December 2019 eruption of Whakaari/White Island from analysis of TROPOMI SO₂ imagery. *Science Advances*, **7**, eabg1218, https://doi.org/10.1126/sciadv.abg1218

Carn, S.A. and Krotkov, N.A. 2016. Ultraviolet satellite measurements of volcanic ash. *In*: Mackie, S., Cashman, K., Ricketts, H., Rust, A. and Watson, M. (eds) *Volcanic Ash: Hazard Observation*. Elsevier, 217–231, https://doi.org/10.1016/B978-0-08-100405-0.00018-5

Carn, S.A., Clarisse, L. and Prata, A.J. 2016. Multi-decadal satellite measurements of global volcanic degassing. *Journal of Volcanology and Geothermal Research*, **311**, 99–134, https://doi.org/10.1016/j.jvolgeores.2016.01.002

Carn, S.A., Fioletov, V.E., Mclinden, C.A., Li, C. and Krotkov, N.A. 2017. A decade of global volcanic SO₂ emissions measured from space. *Scientific Reports*, **7**, 1–12, https://doi.org/10.1038/srep44095

Clarisse, L., Coheur, P.-F., Chefdeville, S., Lacour, J.-L., Hurtmans, D. and Clerbaux, C. 2011. Infrared satellite observations of hydrogen sulfide in the volcanic plume of the August 2008 Kasatochi eruption. *Geophysical Research Letters*, **38**, https://doi.org/10.1029/2011GL047402

Cole, P.D., Robertson, R.E.A., Fedele, L. and Scarpati, C. 2019. Explosive activity of the last 1000 years at La Soufrière, St Vincent, Lesser Antilles. *Journal of Volcanology and Geothermal Research*, **371**, 86–100, https://doi.org/10.1016/j.jvolgeores.2019.01.002

de Graaf, M., Sihler, H., Tilstra, L.G. and Stammes, P. 2016. How big is an OMI pixel? *Atmospheric Measurement Techniques*, **9**, 3607–3618, https://doi.org/10.5194/amt-9-3607-2016

Dualeh, E.W., Ebmeier, S.K. *et al.* 2023. Rapid pre-explosion increase in dome extrusion rate at La Soufrière, St. Vincent quantified from Synthetic Aperture Radar backscatter. *Earth and Planetary Science Letters*, **603**, 117980, https://doi.org/10.1016/j.epsl.2022.117980.

Duffell, H.J., Oppenheimer, C., Pyle, D.M., Galle, B., McGonigle, A.J.S. and Burton, M.R. 2003. Changes in gas composition prior to a minor explosive eruption at Masaya volcano, Nicaragua. *Journal of Volcanology and Geothermal Research*, **126**, 327–339, https://doi.org/10.1016/S0377-0273(03)00156-2

Fedele, L., Cole, P.D., Scarpati, C. and Robertson, R.E.A. 2021. Petrological insights on the last 1000 years of explosive activity at La Soufrière, St. Vincent (Lesser Antilles). *Lithos*, **392–393**, 106150, https://doi.org/10.1016/j.lithos.2021.106150

Fischer, T.P., Morrissey, M.M., Lucía Calvache, V.M., Gómez, M.D., Torres, C.R., Stix, J. and Willliams, S.N. 1994. Correlations between SO₂ flux and long-period seismicity at Galeras Volcano. *Nature*, **368**, 135–137, https://doi.org/10.1038/368135a0

Gansecki, C., Lee, R.L., Shea, T., Lundblad, S.P., Hon, K. and Parcheta, C. 2019. The tangled tale of Kīlauea's 2018 eruption as told by geochemical monitoring. *Science (New York, NY)*, **366**, eaaz0147, https://doi.org/10.1126/science.aaz0147

Global Volcanism Project 2021. Report on Soufriere St. Vincent (Saint Vincent and the Grenadines). *In*: Bennis, K.L. and Venzke, E. (eds) *Bulletin of the Global Volcanism Network*. Smithsonian Institution, **46**, 5, https://doi.org/10.5479/si.GVP.BGVN202105-360150

Hedelt, P., Efremenko, D.S., Loyola, D.G., Spurr, R. and Clarisse, L. 2019. Sulfur dioxide layer height retrieval from Sentinel-5 Precursor/TROPOMI using FP_ILM. *Atmospheric Measurement Techniques*, **12**, 5503–5517, https://doi.org/10.5194/amt-12-5503-2019

Hoshyaripour, G., Hort, M. and Langmann, B. 2012. How does the hot core of a volcanic plume control the sulfur speciation in volcanic emission? *Geochemistry, Geophysics, Geosystems*, **13**, https://doi.org/10.1029/2011GC004020

Joseph, E.P., Camejo-Harry, M. *et al.* 2022. Responding to eruptive transitions during the 2020–2021 eruption of La Soufrière volcano, St. Vincent. *Nature Communications*, **13**, 4129, https://doi.org/10.1038/s41467-022-31901-4

Karagulian, F., Clarisse, L., Clerbaux, C., Prata, A.J., Hurtmans, D. and Coheur, P.F. 2010. Detection of volcanic SO₂, ash, and H₂SO₄ using the Infrared Atmospheric Sounding Interferometer (IASI). *Journal of Geophysical Research: Atmospheres*, **115**, https://doi.org/10.1029/2009JD012786

Krotkov, N.A., Krueger, A.J. and Bhartia, P.K. 1997. Ultraviolet optical model of volcanic clouds for remote sensing of ash and sulfur dioxide. *Journal of Geophysical Research: Atmospheres*, **102**, 21891–21904, https://doi.org/10.1029/97JD01690

Krueger, A.J. 1983. Sighting of El Chichón sulfur dioxide clouds with the Nimbus 7 Total Ozone Mapping Spectrometer. *Science*, **220**, https://doi.org/10.1126/science.220.4604.1377

Levelt, P.F., van den Oord, G.H.J. *et al.* 2006. The ozone monitoring instrument. *IEEE Transactions on Geoscience and Remote Sensing*, **44**, 1093–1101, https://doi.org/10.1109/TGRS.2006.872333

Met Office 2015. *Cartopy: A Cartographic Python Library with a Matplotlib Interface.*

Moxnes, E.D., Kristiansen, N.I., Stohl, A., Clarisse, L., Durant, A., Weber, K. and Vogel, A. 2014. Separation of ash and sulfur dioxide during the 2011 Grímsvötn eruption. *Journal of Geophysical Research: Atmospheres*, **119**, 7477–7501, https://doi.org/10.1002/2013JD021129

NASA 2002. Shuttle Radar Topography Mission (SRTM) Elevation Dataset, https://doi.org/10.5066/F7PR7TFT

Oppenheimer, C., Scaillet, B. and Martin, R.S. 2011. Sulfur degassing from volcanoes: source conditions, surveillance, plume chemistry and earth system impacts. *Reviews in Mineralogy and Geochemistry*, **73**, 363–421, https://doi.org/10.2138/rmg.2011.73.13

Palmer, P.I., Jacob, D.J. *et al.* 2001. Air mass factor formulation for spectroscopic measurements from satellites: application to formaldehyde retrievals from the Global

Ozone Monitoring Experiment. *Journal of Geophysical Research: Atmospheres*, **106**, 14539–14550, https://doi.org/10.1029/2000JD900772

Pardini, F., Burton, M., de' Michieli Vitturi, M., Corradini, S., Salerno, G., Merucci, L. and Di Grazia, G. 2017. Retrieval and intercomparison of volcanic SO_2 injection height and eruption time from satellite maps and ground-based observations. *Journal of Volcanology and Geothermal Research*, **331**, 79–91, https://doi.org/10.1016/j.jvolgeores.2016.12.008

Pardini, F., Burton, M., Arzilli, F., La Spina, G. and Polacci, M. 2018. SO_2 emissions, plume heights and magmatic processes inferred from satellite data: the 2015 Calbuco eruptions. *Journal of Volcanology and Geothermal Research*, **361**, 12–24, https://doi.org/10.1016/j.jvolgeores.2018.08.001

Platt, U. and Stutz, J. 2008. *In*: Guzzi, R., Lanzerotti, L.J., Imboden, D. and Platt, U. (eds) *Differential Optical Absorption Spectroscopy*, 1st edn. Springer, https://doi.org/10.1007/978-3-540-75776-4

Platt, U., Bobrowski, N. and Butz, A. 2018. Ground-based remote sensing and imaging of volcanic gases and quantitative determination of multi-species emission fluxes. *Geosciences (Switzerland)*, **8**, https://doi.org/10.3390/geosciences8020044

Prata, A.J. and Kerkmann, J. 2007. Simultaneous retrieval of volcanic ash and SO_2 using MSG-SEVIRI measurements. *Geophysical Research Letters*, **34**, https://doi.org/10.1029/2006GL028691

Pyle, D.M., Barclay, J. and Armijos, M.T. 2018. The 1902–3 eruptions of the Soufrière, St Vincent: Impacts, relief and response. *Journal of Volcanology and Geothermal Research*, **356**, 183–199, https://doi.org/10.1016/j.jvolgeores.2018.03.005

Queißer, M., Burton, M. *et al.* 2019. TROPOMI enables high resolution SO_2 flux observations from Mt. Etna, Italy, and beyond. *Scientific Reports*, **9**, 1–12, https://doi.org/10.1038/s41598-018-37807-w

Robock, A. 2000. Volcanic eruptions and climate. *Reviews of Geophysics*, **38**, 191–219, https://doi.org/10.1029/1998RG000054

Salerno, G.G., Burton, M., Di Grazia, G., Caltabiano, T. and Oppenheimer, C. 2018. Coupling between magmatic degassing and volcanic tremor in basaltic volcanism. *Frontiers in Earth Science*, **6**, https://doi.org/10.3389/feart.2018.00157

Sigmarsson, O., Haddadi, B., Carn, S., Moune, S., Gudnason, J., Yang, K. and Clarisse, L. 2013. The sulfur budget of the 2011 Grímsvötn eruption, Iceland. *Geophysical Research Letters*, **40**, 6095–6100, https://doi.org/10.1002/2013GL057760

Sparks, R.S.J. 2003. Forecasting volcanic eruptions. *Earth and Planetary Science Letters*, **210**, 1–15, https://doi.org/10.1016/S0012-821X(03)00124-9

Sparks, R.S.J. and Aspinall, W.P. 2004. Volcanic activity: Frontiers and challenges in forecasting, prediction and risk assessment. *American Geophysical Union Monographs*, **150**, 359–373, https://doi.org/10.1029/150GM28

Sparks, R.S.J. and Wilson, L. 1982. Explosive volcanic eruptions – V. Observations of plume dynamics during the 1979 Soufriere eruption, St Vincent. *Geophysical Journal International*, **69**, 551–570, https://doi.org/10.1111/j.1365-246X.1982.tb04965.x

Sparks, S.R.J., Aspinall, W.P., Barclay, J., Renfrew, I., Contreras-Arratia, R. and Stewart, R. 2023. Analysis of magma flux and eruption intensity during the 2021 explosive activity at the Soufrière of St Vincent, West Indies. *Geological Society, London, Special Publications*, **539**, https://doi.org/10.1144/SP539-2022-286

Stein, A.F., Draxler, R.R., Rolph, G.D., Stunder, B.J.B., Cohen, M.D. and Ngan, F. 2015. NOAA's HYSPLIT atmospheric transport and dispersion modeling system. *Bulletin of the American Meteorological Society*, **96**, 2059–2077, https://doi.org/10.1175/BAMS-D-14-00110.1

Stothers, R.B. 2009. Volcanic eruptions and climate change. *In*: Gornitz, V. (ed.) *Encyclopedia of Paleoclimatology and Ancient Environments*. Encyclopedia of Earth Sciences Series, Springer, 947–950, https://doi.org/10.1007/978-1-4020-4411-3_227

Symonds, R.B., Rose, W.I., Bluth, G.J.S. and Gerlach, T.M. 1994. Volcanic-gas studies: methods, results, and applications. *Reviews in Mineralogy*, **30**, 1–66, https://doi.org/10.1515/9781501509674

Theys, N., Campion, R. *et al.* 2013. Volcanic SO_2 fluxes derived from satellite data: a survey using OMI, GOME-2, IASI and MODIS. *Atmospheric Chemistry and Physics*, **13**, 5945–5968, https://doi.org/10.5194/acp-13-5945-2013

Theys, N., De Smedt, I. *et al.* 2017. Sulfur dioxide retrievals from TROPOMI onboard Sentinel-5 Precursor: algorithm theoretical basis. *Atmospheric Measurement Techniques*, **10**, 119–153, https://doi.org/10.5194/amt-10-119-2017

Theys, N., Hedelt, P. *et al.* 2019. Global monitoring of volcanic SO_2 degassing with unprecedented resolution from TROPOMI onboard Sentinel-5 Precursor. *Scientific Reports*, **9**, 1–10, https://doi.org/10.1038/s41598-019-39279-y

Theys, N., Lerot, C. *et al.* 2022. Improved retrieval of SO_2 plume height from TROPOMI using an iterative Covariance-Based Retrieval Algorithm. *Atmospheric Measurement Techniques Discussions*, **2022**, 1–35, https://doi.org/10.5194/amt-2022-148

Varnam, M., Burton, M., Esse, B., Kazahaya, R., Salerno, G., Caltabiano, T. and Ibarra, M. 2020. Quantifying light dilution in ultraviolet spectroscopic measurements of volcanic SO_2 using dual-band modeling. *Frontiers in Earth Science*, **8**, https://doi.org/10.3389/feart.2020.528753

Veefkind, J.P., Aben, I. *et al.* 2012. TROPOMI on the ESA Sentinel-5 Precursor: a GMES mission for global observations of the atmospheric composition for climate, air quality and ozone layer applications. *Remote Sensing of Environment*, **120**, 70–83, https://doi.org/10.1016/j.rse.2011.09.027

von Glasow, R., Bobrowski, N. and Kern, C. 2009. The effects of volcanic eruptions on atmospheric chemistry. *Chemical Geology*, **263**, 131–142, https://doi.org/10.1016/j.chemgeo.2008.08.020

Wilson, T.M., Stewart, C. *et al.* 2012. Volcanic ash impacts on critical infrastructure. *Physics and Chemistry of the Earth*, **45–46**, 5–23, https://doi.org/10.1016/j.pce.2011.06.006

Woodhouse, M.J., Phillips, J.C. and Hogg, A.J. 2016. Unsteady turbulent buoyant plumes. *Journal of Fluid Mechanics*, **794**, 595–638, https://doi.org/10.1017/jfm.2016.101